

RESEARCH ARTICLE

Histone H1 eviction by the histone chaperone SET reduces cell survival following DNA damage

Imke K. Mandemaker^{1,*}, Di Zhou¹, Serena T. Bruens¹, Dick H. Dekkers², Pernette J. Verschure³, Raghu R. Edupuganti^{4,‡}, Eran Meshorer^{4,5}, Jeroen A. A. Demmers² and Jurgen A. Marteijn^{1,§}

ABSTRACT

Many chromatin remodeling and modifying proteins are involved in the DNA damage response, where they stimulate repair or induce DNA damage signaling. Interestingly, we identified that downregulation of the histone H1 (H1)-interacting protein SET results in increased resistance to a wide variety of DNA damaging agents. We found that this increased resistance does not result from alleviation of an inhibitory effect of SET on DNA repair but, rather, is the consequence of a suppressed apoptotic response to DNA damage. Furthermore, we provide evidence that the histone chaperone SET is responsible for the eviction of H1 from chromatin. Knockdown of H1 in SET-depleted cells resulted in re-sensitization of cells to DNA damage, suggesting that the increased DNA damage resistance in SET-depleted cells is the result of enhanced retention of H1 on chromatin. Finally, clonogenic survival assays showed that SET and p53 act epistatically in the attenuation of DNA damage-induced cell death. Taken together, our data indicate a role for SET in the DNA damage response as a regulator of cell survival following genotoxic stress.

This article has an associated First Person interview with the first author of the paper.

KEY WORDS: DNA damage, Histone H1, Histone chaperone, SET

INTRODUCTION

The integrity of DNA is constantly challenged by exogenous and endogenous DNA-damaging agents that can cause a wide variety of DNA lesions. Cells have evolved a sophisticated network of different pathways, collectively named the DNA damage response (DDR) (Jackson and Bartek, 2009), to properly respond to genomic insults. The DDR involves activation of different DNA repair mechanisms, each endowed to detect and remove specific subsets of

DNA lesions (Hoeijmakers, 2009), and a complex damage signaling network that controls cell cycle progression, transcriptional reprogramming and apoptosis. The DDR is active in different cell types, genomic environments and cell cycle phases, but always acts in the context of chromatin. Chromatin is considered to impose an important constraint on how easy it is for repair proteins to access DNA lesions. However, it has also been shown to serve as a crucial regulatory platform for many DNA damage signaling events (Smerdon, 1991; Riley et al., 2008; Soria et al., 2012; Mandemaker et al., 2014). In accordance with the important role of chromatin in the DDR, many proteins have been implicated in regulating chromatin changes and plasticity in response to DNA damage, including ATP-dependent chromatin remodelers, histone-modifying enzymes and histone chaperones (Escargueil et al., 2008; Lans et al., 2012; Soria et al., 2012; Dinant et al., 2013; Mandemaker et al., 2014). For example, the DDR kinases ATM and ATR are important for production of phosphorylated histone H2AX (γ H2AX) during the DDR, which stimulates the assembly of repair complexes and is involved in the regulation of cell cycle checkpoints and transcription (Yuan et al., 2010). Deletion of the BRG1 and BRM catalytic ATPase subunits of the SWI/SNF chromatin remodeling complex also interferes with the induction of γ H2AX and consequently impairs repair (Park et al., 2006). Furthermore, histone chaperones are involved in the DDR, acting to assemble and disassemble nucleosomes during repair processes (Mandemaker et al., 2014). The histone chaperone FACT has been shown to stimulate exchange of histones H2A and H2B at sites of UV-induced DNA damage, thereby promoting transcriptional restart after UV irradiation (Dinant et al., 2013). Alternatively, histone chaperones may also replace histones with specific histone variants. For example, HIRA deposits newly synthesized histone H3.3 onto chromatin at damaged sites (Adam et al., 2013).

Thus far, most research has focused on the remodeling, modification and exchange of core histones and their variants. However, increasing evidence shows that the linker histone H1 (H1) also plays an important role in the DDR, even though its exact role remains elusive. Although it has been shown that a 50% reduction in H1 levels results in enhanced H2AX and Chk1 (also known as CHEK1) phosphorylation and increased survival after DNA damage in mouse embryonic stem cells (mESCs) (Murga et al., 2007), it has also been observed that H1-depleted cells are more sensitive to genotoxic agents (Nishiyama et al., 2009). More recently, a more specific DDR-related role for H1, as a ubiquitin substrate in the RNF8/RNF168 pathway, has been described (Thorslund et al., 2015; Mandemaker et al., 2017). Ubiquitylation of H1 leads to the recruitment RNF168, triggering ubiquitylation of core histones and eventually leading to the binding of downstream DDR factors such as TP53BP1 and BRCA1 (Thorslund et al., 2015; Mandemaker et al., 2017). Taken together, these data indicate that H1 is an important regulator of the DDR.

¹Erasmus MC, University Medical Center Rotterdam, Department of Molecular Genetics, OncoCode Institute, Wytemaweg 80, 3015 CN Rotterdam, The Netherlands.

²Proteomics Center, Erasmus University Medical Center, 3015 CN Rotterdam, The Netherlands. ³Swammerdam Institute for Life Sciences, University of Amsterdam, 1098 XH Amsterdam, The Netherlands. ⁴The Department of Genetics, The Alexander Silberman Institute of Life Sciences, The Hebrew University of Jerusalem, Edmond J. Safra campus, 91904 Jerusalem, Israel. ⁵The Edmond and Lily Safra Center for Brain Sciences, The Hebrew University of Jerusalem, Jerusalem 91904, Israel.

*Present address: Biomedical Center, Physiological Chemistry, Ludwig-Maximilians-Universität München, Planegg-Martinsried, Germany. †Present address: Department of Human Genetics, University of Miami Miller School of Medicine, Sylvester Comprehensive Cancer Center, Biomedical Research Building, Room 719, 1501 NW 10th Avenue, Miami, FL 33136, USA.

§Author for correspondence (J.Marteijn@erasmusmc.nl)

✉ Author for correspondence (J.Marteijn@erasmusmc.nl)

© I.K.M., 0000-0002-5386-6276; J.A.M., 0000-0001-9321-518X

In this study, we set out to further investigate the role, and underlying regulatory mechanism, of H1 involvement in the DDR. Among many other chromatin-associated factors, we identified the proto-oncogenic protein SET (also known as TAF1) as an H1-interacting protein. Because SET was previously identified as an H1 chaperone (Kato et al., 2011), we focused on the role of SET in the DDR. SET was first identified as an inhibitor of protein phosphatase 2A (PP2A) (Li et al., 1995) and is a negative regulator of c-Myc and other pro-survival pathways (Arnold and Sears, 2008). In addition, SET inhibits the pro-apoptotic NME1 (also known as NDK A) hexamer complex, involved in the suppression of tumor metastasis (Fan et al., 2003). In line with these functions, overexpression of SET is involved in the initiation of various types of cancer (Christensen et al., 2011; Hung and Chen, 2017). SET also has diverse functions in transcription; as part of the INHAT complex it represses transcription by inhibiting the activity of the CBP/p300 transcriptional co-activators (Seo et al., 2001; Loven et al., 2003), but it also stimulates transcription by remodeling chromatin (Okuwaki and Nagata, 1998; Gamble et al., 2005). In addition, SET directly binds to p53 (also known as TP53) in unstressed conditions, thereby repressing its activity (Kim et al., 2012; Wang et al., 2016).

Here, we show that downregulation of SET enhances resistance to a wide variety of genotoxic agents, without stimulating DNA repair. Using different imaging techniques, we show that SET is involved in the dissociation of H1 from chromatin, suggesting that depletion of SET results in increased H1 binding to chromatin. Knockdown of H1 reverses the increased DNA damage resistance induced by SET depletion, indicating that this effect is directly caused by the H1 chaperone activity of SET. Furthermore, survival experiments indicate that p53 and SET are epistatic for the increased resistance to genotoxic stress. Together, our data suggest that both histone H1 and SET, like p53, have an important role in the regulation of cellular survival after DNA damage.

RESULTS

SET depletion leads to DNA damage resistance

To address the role of H1, and more specifically its chromatin deposition, during the DDR (Murga et al., 2007; Nishiyama et al., 2009), we set out to identify factors involved in H1 regulation using quantitative proteomics on GFP-tagged histone H1.2 (H1.2) pulldown samples. In addition to core histones and chromatin involved factors, we identified the oncoprotein SET, a suggested H1

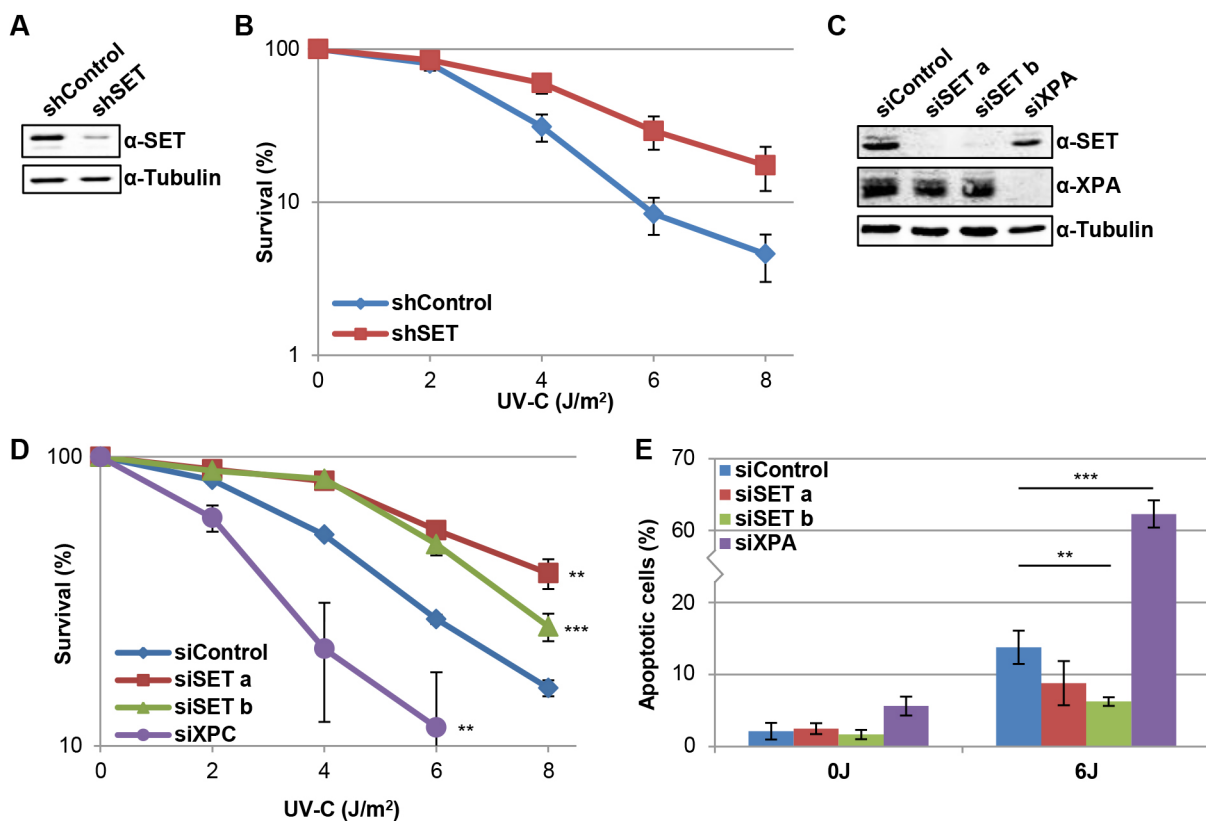


Fig. 1. Depletion of SET leads to enhanced cellular survival after UV-induced DNA damage. (A) Western blot (representative of $n=3$ experiments) showing expression levels of SET in mESCs expressing shControl or shSET. Tubulin is used as a loading control. (B) Clonogenic UV survival of mESCs expressing shControl or shSET. The relative colony survival, normalized to 100% at 0 J/m², is plotted against the UV-C dose. Data are mean \pm s.e.m. $n=3$ individual experiments. Two-sided paired t -test of area under the curve (AUC), $P=0.117$. (C) Western blots (representative of $n=5$ experiments) of whole cell extracts from U2OS cells, using antibodies against SET and XPA, showing the knockdown efficiency of the indicated siRNAs. Tubulin is used as a loading control. (D) Clonogenic UV survival of U2OS cells transfected with either siControl, siXPC, siSETa or siSETb. The colony survival is normalized to 100% at respective 0 J/m² conditions and plotted against the UV-C dose. Data are mean \pm s.e.m. $n\geq 3$ individual experiments. siControl vs siSETa, $P=0.0037$; siControl vs siSETb, $P=0.0002$; siControl vs siXPC, $P=0.0036$ (one-way ANOVA with Dunnett's test of AUC). (E) Quantification of apoptotic U2OS cells, after mock (0 J/m²; 0J) or UV-irradiation (6 J/m²; 6J), as determined by assaying cytochrome c release. Apoptosis assays were executed in the presence of caspase inhibitor Q-VD-OPH (20 μ M), which arrests the apoptotic process after release of cytochrome c , resulting in the accumulation of apoptotic cells. Data show mean \pm s.e.m., $n>5$. siControl vs siSETa, $P=0.0817$; siControl vs siSETb, $P=0.0020$; siControl vs siXPC $P<0.0001$ (one-way ANOVA with Dunnett's test). ** $P<0.01$, *** $P<0.001$.

chaperone (Kato et al., 2011; Zhang et al., 2015), as an H1 interactor (Table S1) (Kato et al., 2011; Zhang et al., 2015).

To address the involvement of SET in the DDR, we performed clonogenic survival experiments following UV exposure of mESCs in which SET was knocked down by stable shRNA expression (Fig. 1A) (Edupuganti et al., 2017). Surprisingly, upon SET knockdown, cells were less sensitive to UV irradiation than cells expressing a non-targeting control shRNA (Fig. 1B). This effect was not specific for mESCs, as increased UV resistance was also observed in U2OS cells following siRNA-mediated SET knockdown (Fig. 1C, D). Depletion of the essential nucleotide excision repair (NER) gene *XPC* resulted in the expected increase in UV sensitivity (Fig. 1D). The DNA damage resistance induced by SET knockdown was in a large part caused by a reduced level of UV damage-induced apoptosis, as determined by measuring cytochrome *c* release from mitochondria (Fig. 1E; Fig. S1). As expected, a UV-induced increase in the percentage of cells undergoing apoptosis was observed 32 h after UV irradiation (Dunkern et al., 2001). Induction of apoptosis was enhanced in XPA-depleted cells, whereas a ~50% reduction in UV damage-induced apoptosis was observed following siRNA-mediated SET knockdown (Fig. 1E).

Increased survival of SET-depleted cells is independent of DNA repair

The increase in UV resistance upon SET knockdown could be explained by changes in DNA replication, as UV-induced photoproducts can block replication, causing replication stress and affecting cellular survival. To test this, we studied whether SET influences the cell cycle. However, we found no difference in cell cycle distribution upon SET depletion in either mock- or UV-treated cells (Fig. 2A; Fig. S2A), indicating that the observed higher UV-resistance in SET-depleted cells was not a consequence of changes in replication rate.

Resistance to UV irradiation could also be caused by a change in the efficiency of the repair of UV-induced lesions through NER. NER is initiated by the recognition of lesions either by global genome repair (GG-NER) proteins (including XPC and the DDB complex) or, when lesions are in actively transcribed genes, by the stalling of RNA polymerase II (termed transcription-coupled repair or TC-NER) (Sugasawa, 2016). After damage recognition, the NER reaction proceeds with helix unwinding and lesion verification, which are similar in both GG-NER and TC-NER. Subsequently, a 25–30 nucleotide piece of DNA containing the damaged nucleotide

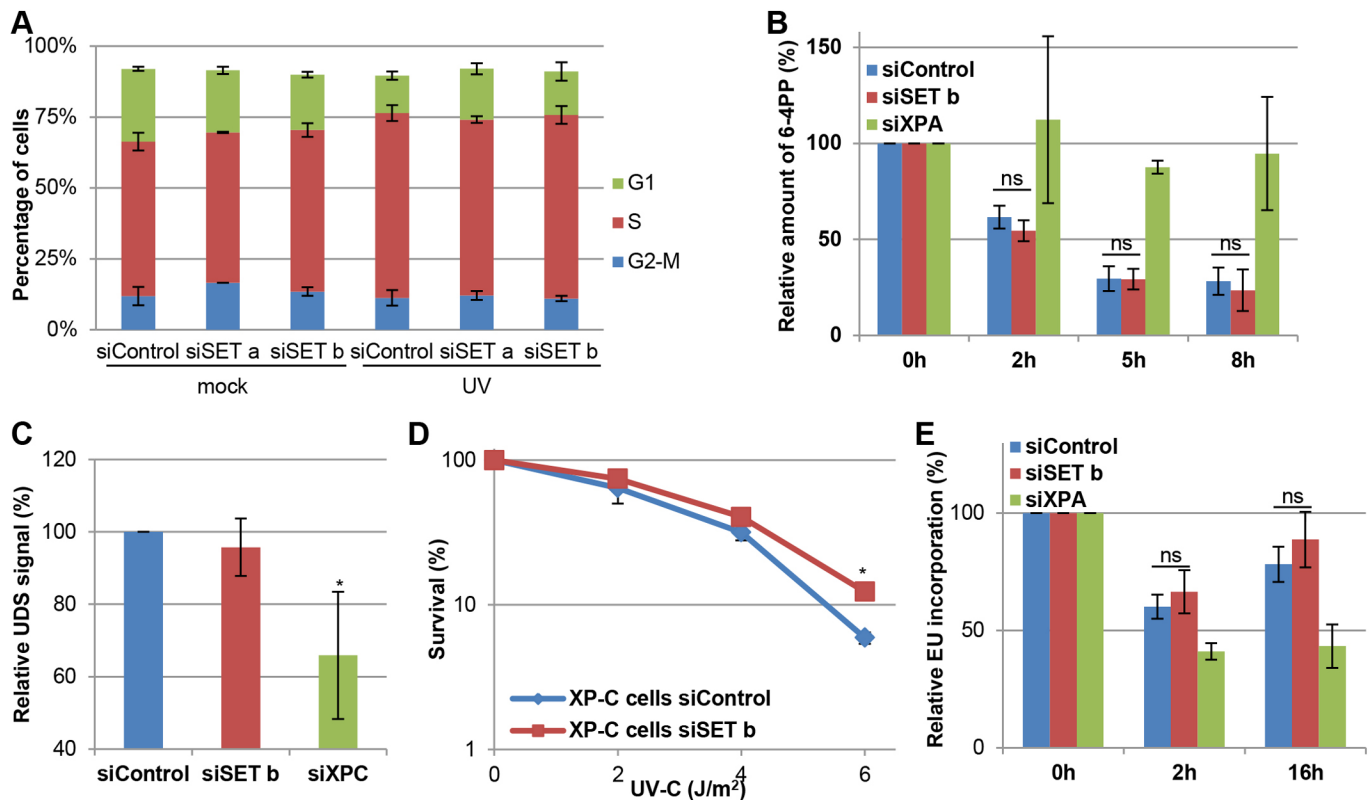


Fig. 2. Depletion of SET does not affect cell cycle progression or NER efficiency. (A) Cell cycle distribution analyzed by EdU (10 μ M) incorporation and DAPI (1 μ g/ml) staining of U2OS cells transfected with the indicated siRNAs followed by FACS analysis. Cells were analyzed 16 h after mock or 2 J/m^2 UV treatment. Data show mean \pm s.e.m. $n=2$ individual experiments. (B) Quantification of relative amount of 6–4PP at different timepoints after UV irradiation (10 J/m^2) of U2OS cells. Amount of 6–4PP was quantified by immunofluorescence intensity and data was normalized to the 0 h timepoint for each cell line. Data show mean \pm s.e.m. $n=3$ (with ≥ 100 cells per experiment). siControl vs siSET b: 2 h, $P=0.0941$; 5 h, $P=0.9644$; 8 h, $P=0.6384$; ns, not significant (two-sided paired *t*-test). (C) UDS measured by the incorporation of EdU (20 μ M) in non-S-phase C57RO cells after UV irradiation (16 J/m^2). UDS levels in siControl cells were set as 100%. Data show mean \pm s.e.m. $n=2-3$ experiments, with ≥ 100 cells analyzed per experiment. siControl vs siSET b, $P=0.8057$; siControl vs siXPC, $P=0.0150$ (one-way ANOVA with Dunnett's test). (D) Clonogenic UV-survival in XP4PA (XPC-deficient) cells transfected with the indicated siRNAs. The relative percentage colony survival, normalized to 0 J/m^2 , is plotted against the UV-C dose. Data show mean \pm s.e.m. $n=2$ independent experiments. $P=0.0566$, one-sided paired *t*-test of area under the curve; $P=0.0308$, one-sided paired *t*-test of 6 J/m^2 treatment data. (E) RNA synthesis in U2OS cells, as determined by quantification of EU (100 μ M) incorporation. Amount of EU incorporation 2 and 16 h after UV treatment is normalized to amount in untreated cells. Data are mean \pm s.e.m. $n\geq 2$ independent experiments ($n>75$ cells per experiment). siControl vs siSETb at 2 h, $P=0.5404$; siControl vs siSETb at 16 h, $P=0.4081$ (two-sided *t*-test). * $P<0.05$; ns, not significant.

is removed (Oksenysh and Coin, 2010; Fagbemi et al., 2011; Li et al., 2015; Martejn et al., 2015), the resulting single-stranded DNA gap is filled by DNA polymerases and the nicks are sealed (Ogi et al., 2010). We tested whether SET influences the efficiency of repair of UV-induced lesions by measuring NER activity. First, we quantified the removal of UV-induced 6–4 photoproducts (6–4PPs) by NER. No change in the induction or removal of UV-induced 6–4PP lesions was observed in SET-depleted cells compared to control cells (Fig. 2B; Fig. S2B), whereas a clear decrease in 6–4PP removal was observed in XPA-depleted cells (Fig. 2B). In line with this, no difference in unscheduled DNA synthesis (UDS) (Limsirichaikul et al., 2009), a measure of the final gap-filling step of NER, was observed following SET knockdown, whereas depletion of XPC, as expected, led to a decrease in UDS signal (Fig. 2C). Taken together, these findings show that NER activity is not affected by SET depletion, and indicates that SET depletion-mediated resistance is not caused by increased repair activity. To further corroborate this we performed clonogenic survival assays in XP-C cells, which are deficient in GG-NER. Although XP-C cells are very sensitive to UV irradiation, we still observed increased survival in SET-depleted cells (Fig. 2D), indicating that the enhanced survival is independent of repair. Because the aforementioned assays mainly monitor the activity of

GG-NER, we also tested whether SET influenced TC-NER. TC-NER activity was assessed by the recovery of RNA synthesis (RRS) after UV-induced transcription inhibition. To do this, we quantified transcription rates by pulse labeling with the uridine analog EU (Nakazawa et al., 2010). Although we saw a clear reduction in RRS at 16 h after UV irradiation of XPA-depleted cells deficient in TC-NER, we observed no difference in RRS between control and SET-depleted cells (Fig. 2E), indicating that TC-NER efficiency is not affected by SET.

Previously, it was shown that SET affects cell survival after DNA double-strand break (DSB) induction (Kalouisi et al., 2015). In line with this, we observed that SET knockdown also led to increased resistance to ionizing radiation in both U2OS (Fig. 3A) and mESCs (Fig. S3A). In response to DSBs, SET densifies chromatin via KAP1 (also known as TRIM28)-dependent recruitment of heterochromatin protein 1 (HP1), leading to a shift in the balance between homologous recombination (HR) and non-homologous end joining (NHEJ) (Kalouisi et al., 2015). However, NHEJ and HR are not the major repair pathways involved in UV survival (Hoeijmakers, 2001), and therefore it is unlikely that the observed UV resistance in SET-depleted cells is caused by this mechanism. Accordingly, KAP1-depleted cells showed similar survival to control cells upon UV exposure, whereas

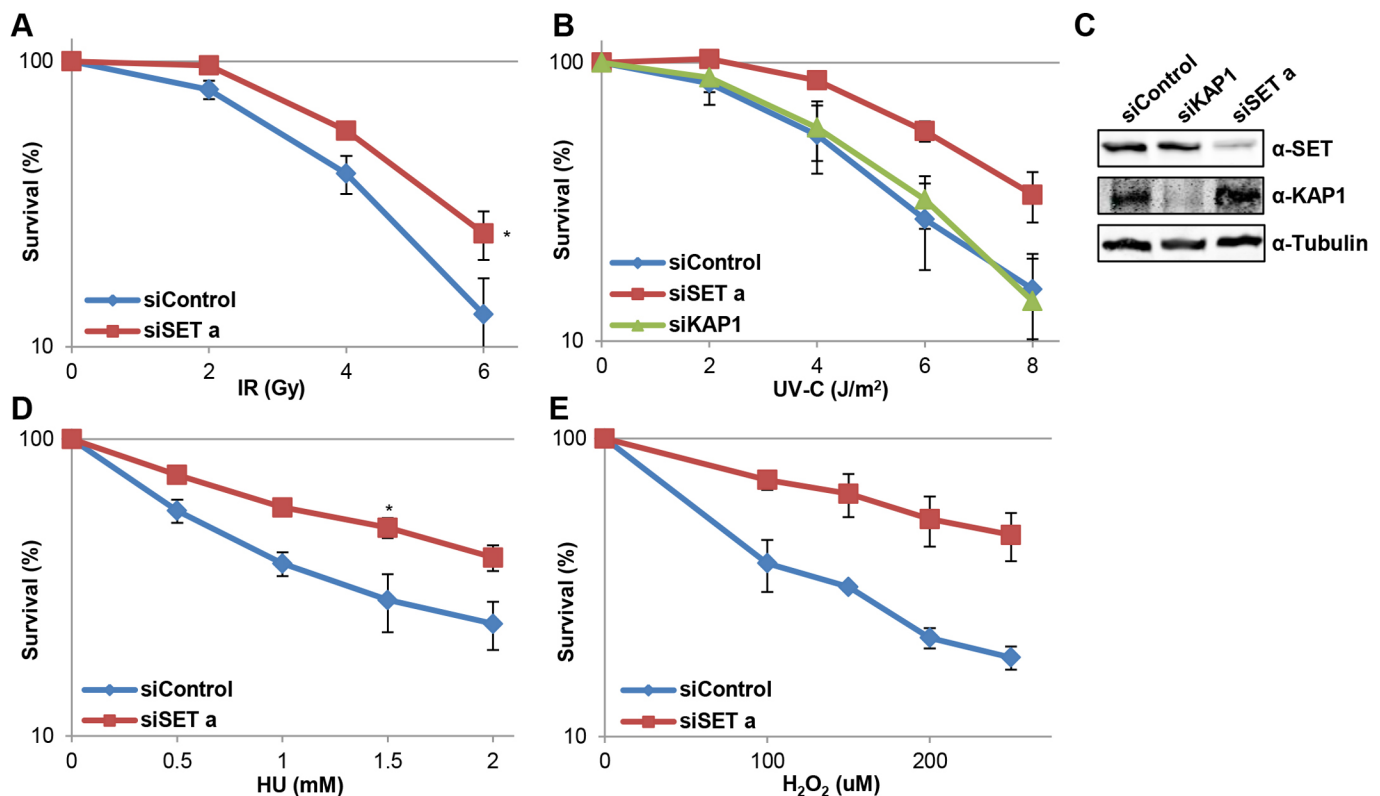


Fig. 3. SET depletion leads to increased resistance to a wide variety of DNA damaging agents. (A) Colony survival of U2OS cells transfected with siControl or siSETa and treated with ionizing irradiation. Relative colony survival, normalized to 100% in untreated samples, is plotted against the treatment dose. Data are mean±s.e.m. $n=3$ experiments, $P=0.0365$ [one-sided paired t -test of area under the curve (AUC)]. (B) Clonogenic survival experiments of U2OS cells transfected with siControl, siSETa or siKAP1 treated with UV-C irradiation. Data are mean±s.e.m. $n=3$ experiments, normalized to 100% in untreated samples. siControl vs siSETa, $P=0.0568$; siControl vs siKAP1, $P=0.8815$ (one-way ANOVA with Sidak's test of AUC). (C) Western blot of whole-cell extract from U2OS cells showing knockdown efficiency of the depicted siRNAs. Blots are stained with antibodies against SET, KAP1 and tubulin (loading control), and are representative of $n=3$ independent experiments. (D) Clonogenic survival of U2OS cells transfected with the indicated siRNAs treated with HU. Relative colony survival was normalized to 100% in non-treated conditions. Data are mean±s.e.m. $n=2$ individual experiments. $P=0.0547$, one-sided paired t -test of AUC; $P=0.0359$, one-sided paired t -test of 1.5 mM treatment data. (E) Clonogenic survival of U2OS cells transfected with the indicated siRNAs treated with hydrogen peroxide. Relative colony survival was normalized to 100% in non-treated conditions. Data are mean±s.e.m. $n=2$ individual experiments. $P=0.0984$, one-sided paired t -test of AUC; $P=0.0827$, one-sided paired t -test of 200 mM treatment data. * $P<0.05$.

SET-depleted cells were observed to be more resistant (Fig. 3B,C). This implies that enhanced survival of SET-depleted cells is not mediated by KAP1.

Because SET affects survival after UV- (Fig. 1B,D) and ionizing-radiation-induced (Fig. 3A) (Kalousi et al., 2015) DNA damage, we also tested the response of SET-depleted cells to other structurally different types of DNA lesions that are repaired by different repair pathways. To this end, we performed clonogenic survival assays following treatment with hydrogen peroxide and potassium bromate, which mainly induce oxidative base damage (repaired by base excision repair), and with mitomycin C, which creates DNA interstrand cross-links (repaired by the Fanconi anemia pathway). Interestingly, SET knockdown resulted in higher cellular resistance to all tested DNA damaging agents, as well as hydroxyurea (HU)-induced replication stress (Fig. 3; Fig. S3).

Altered DNA damage signaling is not the cause of the enhanced survival of SET-depleted cells

As SET depletion resulted in resistance to a wide variety of DNA damage, it is highly unlikely that the enhanced resistance in SET-depleted cells is the result of enhanced repair. Instead, SET most likely affects a process that is common to the cellular responses elicited by different types of DNA damage. A likely candidate mechanism is DNA damage signaling by phosphorylation of H2AX, as this common and abundant post-translational modification plays an important role in the DDR and is induced by different types of DNA damage (Rogakou et al., 1998; Ward and Chen, 2001; Mogi and Oh, 2006; Hanasoge and Ljungman, 2007; Martejn et al., 2009; Zhang et al., 2016). Furthermore, previous studies have shown that SET depletion resulted in increased γ H2AX signaling following DSB induction (Kalousi et al., 2015). To test whether SET also affects γ H2AX signaling after other types of DNA damage, we studied H2AX phosphorylation following replication stress by blocking replication forks, in an inducible manner, at a defined and traceable single locus (Beuzer et al., 2014). For this purpose, we expressed Lac repressors (LacR) in U2OS cells that harbor an integrated array of 256 repeats of the *lac* operon (*lacO*) (Fig. 4A), resulting in the tethering of LacR to the *lacO* locus and thereby inducing replication stress. At 36 h after transfection of mCherry–LacR, γ H2AX signal was quantified at the *lacO*. We observed a greater than twofold reduction in γ H2AX signal when mCherry–SET–LacR was targeted to the *lacO* compared to when mCherry–LacR was targeted to the *lacO* (Fig. 4A,B). This reduction in γ H2AX signaling was not caused by a reduction in H2AX levels at the *lacO* following SET tethering (Fig. 4C; Fig. S4A).

These findings prompted us to test whether the effect of SET on γ H2AX signaling is the cause of the DNA damage resistance observed following SET depletion. We performed colony survival assays in which H2AX phosphorylation was suppressed by inhibition of the phosphoinositide 3-kinase-like protein kinases ATR, ATM and DNA-PK, which are involved in H2AX phosphorylation (Sirbu and Cortez, 2013; Guleria and Chandna, 2016). As expected, inhibition of these kinases with caffeine (Sarkaria et al., 1999; Block et al., 2004) resulted in sensitization to UV (Rommelaere and Errera, 1972) (Fig. 4D). Importantly, caffeine-treated cells still presented increased resistance to DNA damage upon SET depletion. Furthermore, similar effects of SET depletion on cell survival were observed when ATM and DNA-PK were inhibited with kinase-specific inhibitors (Fig. S4B). In line with these results, siRNA-mediated depletion of H2AX, resulting in the absence of H2AX phosphorylation upon DNA

damage (Fig. 4E), did not affect the SET knockdown-induced UV resistance (Fig. 4F). Taken together, our data suggest that, even though γ H2AX signaling is affected by SET, it is not the cause of the increased survival of SET-depleted cells upon DNA damage.

Enhanced survival of SET-depleted cells is dependent on H1

Remodeling of the chromatin environment is important for a proper DDR (Lans et al., 2012; Polo and Almouzni, 2015), and, interestingly, SET was previously implicated in nucleosome assembly and H1 chaperoning (Kato et al., 2011). More specifically, *in vitro* data indicate that SET mainly plays a role in the eviction of H1 from chromatin (Zhang et al., 2015). To study whether SET has a similar H1-removal function in living cells, we first tested the effect of SET on H1 chromatin binding by performing fluorescence recovery after photo bleaching (FRAP) studies in cells stably expressing GFP–H1.2. In accordance with previous data (Kato et al., 2011; Edupuganti et al., 2017), we observed a slower recovery of the fluorescence intensity of GFP–H1.2 upon SET knockdown (Fig. 5A). The increased immobilized H1 fraction indicates that there was a lower exchange rate of chromatin-bound GFP–H1.2 molecules, which is most likely the result of reduced removal of chromatin-bound H1 molecules. To confirm that SET is mainly involved in the unloading of H1 from chromatin, we tethered mCherry–SET–LacR in *lacO*-array-containing U2OS cells expressing GFP–H1.2, thereby inducing an increase in the local concentration of SET (Fig. 5B). In contrast to mCherry–LacR, tethering mCherry–SET–LacR at the *lacO* resulted in reduced GFP–H1.2 levels (Fig. 5C). A similar experiment with GFP–histone H3, showed that SET tethering had no effect on histone H3 levels, indicating the preference of SET for H1 (Fig. 5D). In line with previous *in vitro* data (Zhang et al., 2015), these *in vivo* imaging experiments show that SET promotes H1 eviction from chromatin (Fig. 5A–C).

This H1-eviction function of SET suggests that SET depletion results in enhanced retention of H1 on chromatin, which subsequently might affect chromatin structure and compaction, or disturb specific transcriptional programs, resulting in the observed increase in cellular survival. A prediction following from this hypothesis is that reduction of H1 levels would block the increased resistance to DNA damage upon SET depletion. To test this, we depleted H1 in the presence or absence of SET. A combination of three different previously published siRNAs was used to target all six canonical H1 variants (Thorslund et al., 2015), and knockdown of H1.2 was confirmed by western blotting (Fig. 5E). Although H1 depletion alone did not affect cellular survival in response to UV-induced DNA damage, it reduced the resistance to UV damage induced by SET knockdown (Fig. 5F; Fig. S5A). Upon oxidative damage, H1 depletion led to higher sensitivity and completely suppressed the increased survival in SET-depleted cells (Fig. S5B). Taken together, this suggests that the increased DNA damage survival observed in SET-depleted cells is mainly caused by enhanced levels of chromatin-bound H1 due to a loss of the H1 chromatin-eviction function of SET.

Previously, it has been shown that enhanced H1 binding at p53-regulated promoters hampers gene expression of p53-regulated genes, thereby inhibiting apoptosis (Nishiyama et al., 2009). As SET-depleted cells displayed enhanced levels of chromatin-bound H1 (Fig. 5A–C) and reduced apoptosis in response to DNA damage (Fig. 1E), we tested whether SET is involved in the DNA damage-induced p53 response. Clonogenic survival experiments show that

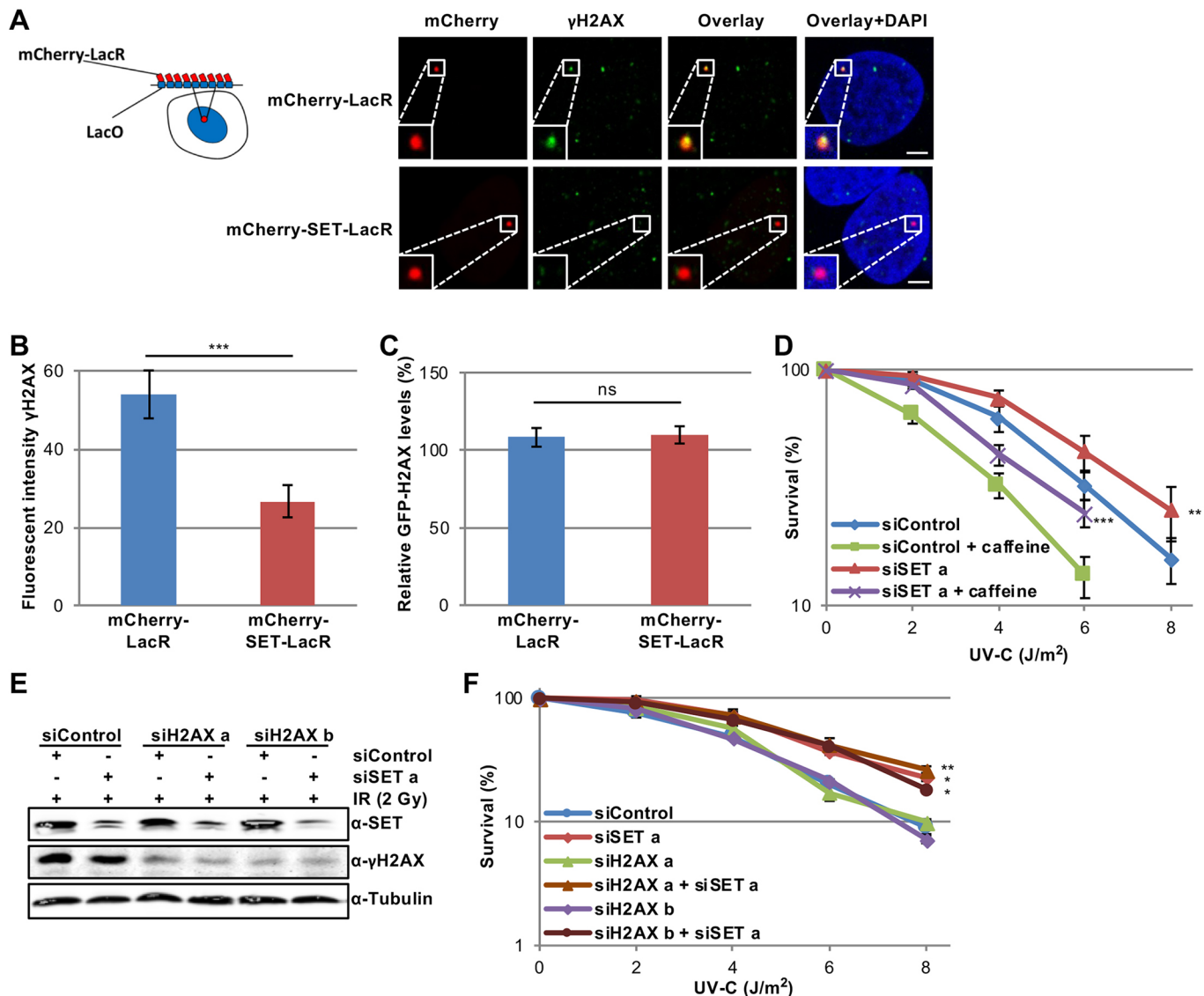


Fig. 4. Altered DNA damage signaling is not the cause of enhanced survival in SET-depleted cells. (A) Diagram and representative immunofluorescence images of U2OS *lacO* cells, containing 256 repeats of the *lac* operon at a defined DNA locus. A Lac repressor specifically binds this operon, allowing the visualization of this locus using mCherry-LacR fusion proteins. γ H2AX signal was determined by antibody staining. Scale bar: 5 μ m. (B) Quantification of a2100 mean γ H2AX signal at the *lacO* of U2OS cells expressing the indicated LacR vectors. Data show mean \pm s.e.m. $n=8$, with 25 cells analyzed per experiment. $P=0.0008$, two-sided paired *t*-test. (C) Quantification of GFP-H2AX levels at the *lacO* of U2OS cells expressing the indicated LacR vectors. GFP-H2AX levels at the *lacO* are normalized to mean levels of GFP-H2AX in the nucleus. Data show mean \pm s.e.m. $n\geq 18$ cells. $P=0.8511$ (two-sided *t*-test). (D) Colony UV survival experiments of U2OS cells treated with caffeine. Percentage of surviving colonies, normalized to 100% at 0 J/m^2 , is plotted against UV-C dose. Data show mean \pm s.e.m. $n=4$ experiments. siControl vs siSETa, $P=0.0014$; siControl+caffeine vs siSETa+caffeine, $P=0.0006$ (one-sided paired *t*-test of area under the curve). (E) Representative western blot ($n=2$ experiments) of whole cell extracts from U2OS cells transfected with the indicated siRNAs, showing the protein levels of SET, γ H2AX and tubulin. One hour prior to lysis, cells were irradiated with 2 Gy (ionizing radiation, IR) to induce γ H2AX signaling. (F) Clonogenic UV survival of cells transfected with siRNAs targeting H2AX. The relative percentage colony survival, normalized to 0 J/m^2 treatment, is plotted against the UV-C dose. Data show mean \pm s.e.m., $n=2$ independent experiments. siControl vs siSETa, $P=0.0432$; siH2AXa vs siH2AXa+siSETa, $P=0.0023$; siH2AXb vs siH2AXb+siSETa, $P=0.0245$ (one-sided paired *t*-test of area under the curve). * $P<0.05$, ** $P<0.01$, *** $P<0.001$; ns, not significant.

knockout of p53 resulted in a similar resistance to DNA damage to that seen upon SET depletion (Fig. 5G,H). Importantly, SET knockdown had no effect on the cell survival in p53-knockout cells, indicating that SET and p53 function in the same pathway. Next, we tested whether SET acted upstream of p53 by stimulating p53-induced gene expression by upregulating H1 unloading at p53-regulated promoters. To do so, we performed reverse transcription quantitative PCR (RT-qPCR) to analyze the levels of the p53-regulated and DNA damage-induced genes *CDKN1A* (encoding p21) and *NOXA* (also known as *PMAIP1*). We did not observe any

significant differences in the induction of *CDKN1A* and *NOXA* upon etoposide treatment after SET depletion (Fig. S5C). These data show that SET knockdown does not hamper the expression of p53-regulated genes, but suggest that SET acts downstream of p53 to prevent apoptosis in response to structurally different types of DNA damage (Figs 1E and 3).

DISCUSSION

In this study, we identified SET as an H1 interactor and showed that SET stimulates chromatin eviction of H1 in living cells, in line with

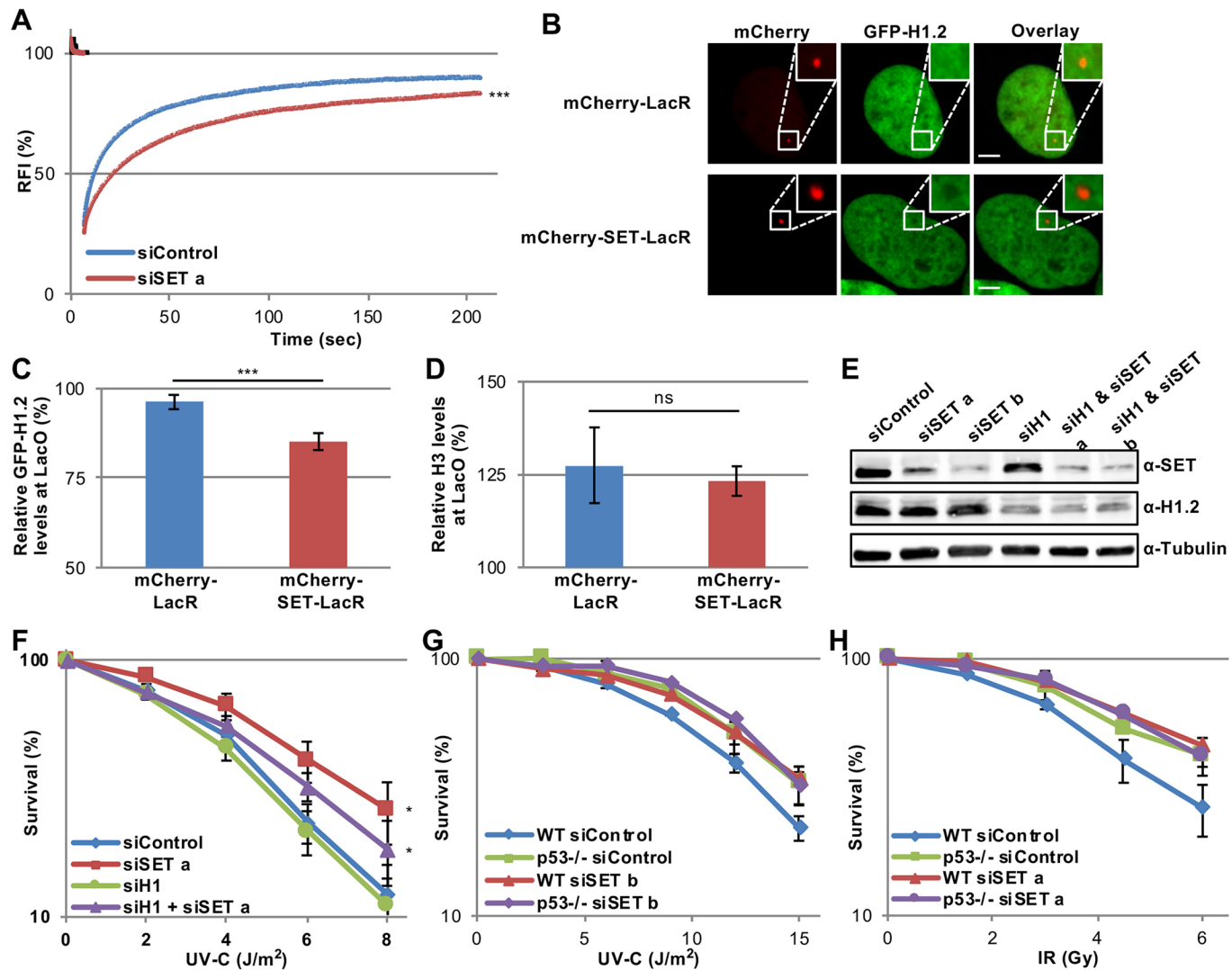


Fig. 5. Higher DNA damage resistance in SET-depleted cells is rescued by H1 downregulation. (A) FRAP analysis of stable GFP–H1.2-expressing U2OS cells transfected with the indicated siRNAs. A small strip spanning the nucleus is bleached and fluorescence recovery measured over time. The fluorescence intensity is normalized to pre-bleach levels. Data show mean \pm s.e.m. $n=3$ experiments (≥ 8 cells/experiment). $P=0.0005$, two-sided paired t -test of area under the curve (AUC). (B) Representative immunofluorescence images of GFP–H1.2-expressing U2OS *lacO* cells transfected with either mCherry–LacR (top panel) or mCherry–SET–LacR (lower panel) vectors. Scale bar: 5 μ m. (C) Quantification of GFP–H1.2 levels at the *lacO*, normalized to the mean GFP–H1.2 signal in the nucleus. Data show mean \pm s.e.m. $n=10$ individual experiments (25 cells/experiment). $P=0.0002$, two-sided paired t -test. (D) Quantification of relative GFP–histone H3 levels at the *lacO* in U2OS cells transfected with the indicated LacR vectors. Data show mean \pm s.e.m., normalized to mean GFP–histone H3 signal in the nucleus. $n=3$ individual experiments (25 cells/experiment). $P=0.7206$ (two-sided paired t -test). (E) Representative western blot of whole cell extracts from U2OS cells, showing the knockdown efficiency siRNAs targeting SET and H1. Tubulin is used as a loading control. (F) Colony survival of U2OS cells transfected with siControl, siSETa and siH1 and treated with UV-C. The relative colony survival, normalized to 100% at 0 J/m^2 , is plotted against the UV-C dose. Data show mean \pm s.e.m. $n=5$ independent experiments. siControl vs siSETa, $P=0.0169$; siH1 vs siH1+siSETa, $P=0.0291$; siControl vs siH1, $P=0.6839$; siControl vs siH1+siSETa, $P=0.7348$ (one-way ANOVA with Sidak's test of AUC). (G) Colony survival of Hct116 wild-type (WT) and $p53^{-/-}$ cells transfected with siControl or siSET and treated with UV-C. The relative colony survival, normalized to 100% in the untreated condition, is plotted against the dose. Data show mean \pm s.e.m., $n=2$. WT siControl vs WT siSETb, $P=0.4285$; WT siControl vs $p53^{-/-}$ siControl, $P=0.2209$; $p53^{-/-}$ siControl vs $p53^{-/-}$ siSETb, $P=0.8248$ (one-way ANOVA with Sidak's test of AUC). (H) Colony survival of Hct116 wild-type (WT) and $p53^{-/-}$ cells transfected with siControl or siSET and treated with ionizing radiation (IR). The relative colony survival, normalized to 100% in the untreated condition, is plotted against the dose. Data show mean \pm s.e.m., $n=2$. WT siControl vs WT siSETa, $P=0.3578$; WT siControl vs $p53^{-/-}$ siControl, $P=0.1339$; $p53^{-/-}$ siControl vs $p53^{-/-}$ siSETa, $P=0.9417$ (one-way ANOVA with Sidak's test of AUC). * $P<0.05$, *** $P<0.001$; ns, not significant.

the H1-chaperoning functions of SET proposed previously (Kato et al., 2011; Zhang et al., 2015). Interestingly, depletion of SET resulted in enhanced cellular resistance to structurally diverse DNA lesions (Fig. 3; Fig. S3) that are targeted by different repair pathways. SET depletion was found to have no effect on the efficacy of repair of either UV-induced lesions (Fig. 2B,C) or DSBs (Kalouisi et al., 2015), suggesting that SET is not a general suppressor of

DNA repair, but more likely functions in a response common to many types of DNA damage, such as DNA damage signaling, chromatin remodeling or the induction of apoptosis.

Previously, it was found that SET functions in the response to DSBs by recruiting KAP1 and HP1 to lesions, thereby affecting DNA damage signaling via phosphorylation of H2AX, and shifting the balance between HR and NHEJ (Kalouisi et al., 2015). In line

with the cellular response of SET-depleted cells to a wide variety of different types of DNA damage in which NHEJ or HR are not expected to play a role, our data show that the increased survival rates of SET-depleted cells upon DNA damage are independent of KAP1 (Fig. 3B) and γ H2AX signaling (Fig. 4D–F). Our data therefore suggest that damage resistance following SET depletion is likely caused by other functions of SET.

Our data show that SET is involved in the eviction of H1 from chromatin and suggest that the histone chaperone activity of SET is necessary for the reduction in cellular survival observed upon DNA damage. Hence, our data are consistent with a model whereby enhanced levels of chromatin-bound H1, caused by SET depletion, prevent efficient induction of cell death in response to DNA damage (Fig. 5F; Fig. S5). Thus far, it is not clear whether the effect of SET knockdown on survival is due to enrichment of H1 throughout the entire chromatin or enrichment of H1 in specific genomic regions of SET activity. One scenario would be that, upon DNA damage, H1 unloading is necessary for transcriptional activation of specific genes involved in apoptosis, which upon SET knockdown are no longer activated. Another possibility is that SET changes the chromatin conformation at sites of DNA damage. Several studies have described a loss of H1 around DSBs (Sellou et al., 2016; Strickfaden et al., 2016; Clouaire et al., 2018). It is possible that SET is involved in actively removing H1 from the regions around the lesions. However, as it is generally assumed that an open chromatin conformation stimulates repair, and thereby survival, and because the presence of SET decreases cellular survival and does not affect repair, this seems a more unlikely scenario. Interestingly, our FRAP studies show a substantial immobilization of H1 upon SET depletion (Fig. 5A), suggesting a genome-wide effect of SET on the chromatin loading of H1.

Our data show that there is no obvious effect on cell survival following SET depletion in the absence of p53 (Fig. 5G,H), indicating that SET is epistatic with the p53 pathway in reducing cell survival following genotoxic stress. In line with the increased chromatin binding of H1 in a genome-wide manner upon SET knockdown, SET does not seem to majorly affect specific p53-regulated transcription upon DNA damage (Fig. S5C) (Nishiyama et al., 2009; Lieberman et al., 2017). This suggests that SET may play a role downstream of p53, for example in stimulating apoptosis upon genotoxic stress. Of note, it was previously shown that, in unstressed conditions, SET can inhibit p53 acetylation, thereby reducing p53 transcriptional activity (Kim et al., 2012; Wang et al., 2016). This indicates that SET may play a multifaceted role in the intricate regulation of p53-mediated transcriptional programs. Moreover, SET has previously been described as an oncogene and is known to have an inhibitory effect on PP2A activity (Li et al., 1995), an important phosphatase implicated in the DDR, which may further confound dissection of the molecular mechanism underlying the role of SET in the DDR (Li et al., 1995).

It is intriguing to note that SET sensitizes cells to DNA damage, as thus far most proteins found to be involved in the DDR, like DNA repair and damage signaling proteins, protect cells against genomic insults. It is possible that our findings represent a mechanism to prevent the formation of mutations following DNA damage, in which SET actively stimulates cell death in cells that cannot reliably repair all DNA lesions, similar to the established pro-apoptotic role of p53 in the DDR (Lieberman et al., 2017). In summary, we have identified a new role for the H1 chaperone SET in the DDR, in which unloading of H1 from chromatin is necessary for the efficient reduction of cellular survival in response to DNA damage.

MATERIALS AND METHODS

Cell lines and cell culture

U2OS, HeLa, Hct116 (obtained from the ATCC) and XP4PA (SV40) cells (Peterson and Legerski, 1991) were cultured in DMEM/F10 medium (Lonza) supplemented with 10% fetal calf serum (FCS, Biowest) and 1% penicillin-streptomycin (PS, P0781 Sigma). C5RO (hTERT) cells (Marteijn et al., 2009) were cultured in F10 supplemented with 15% FCS and 1% PS. mESCs (Edupuganti et al., 2017) were cultured in DMEM/BRL-conditioned medium containing 10% FCS, 1% PS, 1% non-essential amino acids (Lonza), 0.2% β -mercaptoethanol (Invitrogen) and 1000 U/ml leukemia inhibitory factor on gelatin (0.1%) pre-coated dishes. For stable isotope labeling by amino acids in cell culture (SILAC) experiments, cells were cultured for at least ten cell doublings in lysine- and arginine-deficient DMEM (Thermo Fisher Scientific) with 10% dialyzed FCS (Invitrogen), 1% PS, 1% non-essential amino acids and 1% ultraglutamine (200 mM Lonza), supplemented with either ‘light’ [$^{12}\text{C}_6$]lysine (73 $\mu\text{g}/\text{ml}$, Sigma) and [$^{12}\text{C}_6$, $^{14}\text{N}_4$]arginine (42 $\mu\text{g}/\text{ml}$, Sigma) or similar concentrations of ‘heavy’ [$^{13}\text{C}_6$]lysine and [$^{13}\text{C}_6$, $^{15}\text{N}_4$]arginine (Cambridge Isotope Laboratories). All cells were cultured at 37°C and 5% CO_2 in a humidified incubator. For UV treatments, cells were washed with phosphate-buffered saline (PBS) and irradiated using a 254 nm Philips TUV UV-C lamp. Transfections with siRNA were performed using RNAiMax (Invitrogen) according to the manufacturer’s protocol 3 days before treatments. Sequences of siRNAs used were as follows: siControl, 5'-UGGUUUACAUGUCGACUAA-3'; siSETa, 5'-UCUCCAAAGAAUUU-CAUCUGAAU-3'; siSETb, smart pool Dharmacon (L-019586-00-0005); siH1, 5'-CCUUUAAACUCAACAAGAA-3', 5'-CCUCAAACUC-AAC-AAGAA-3' and 5'-CAGUGAAACCCAAAGCAAA-3' (Thorslund et al., 2015); siXPC, 5'-CUGGAGUUUGAGACAUUC-3'; siXPA, 5'-CUGA-UGAUAACACAAGCUUA-3'; siH2AXa, 5'-GUCUCCAGAAGACA-GUGA-3'; siH2AXb, 5'-CAACAAGAGACGCGAAUC-3'; siKAP1, 5'-GCAUGAACCCCUUGUGCUG-3'. Transfections with mCherry–LacR, mCherry–SET–LacR [made from p3'SS-EGFP-dimer lac repressor (Verschure et al., 2005)] and GFP–H2AX (Kimura and Cook, 2001) vectors (2 μg) were performed with Fugene (Promega) according to manufacturer’s protocol 16 h before fixation, unless stated otherwise. For these experiments a U2OS (2-6-3) cell line (David Spector, Cold Spring Harbor Laboratory, New York, USA) containing a chromosomal array of 256 *lacO* repeats and a CFP reporter gene harboring 24 repeats of the MS2 bacteriophage RNA hairpins was used (Janicki et al., 2004). The mCherry–SET–LacR vector was made by ligation of a PCR product containing the SET cDNA into the mCherry–LacR construct digested with *AscI*. The GFP–H1.2 construct was made by cloning a PCR product from an H1.2–FLAG construct (kind gift from Kyosuke Nagata) into a pENTR4-eGFP-C1 vector, followed by an LR clonase reaction to a pLenti-CMV vector (Campeau et al., 2009). Stably expressing GFP–H1.2 cell lines were made by lentiviral transduction. Medium containing lentivirus was harvested 2 days after transient transfection of HEK293 cells with pLenti-CMV-GFP-H1.2, pMDLg/pRRE, pRSV-REV and pMD2.G constructs (Addgene #17452, #12251, #12253 and #12259, respectively). Control (scrambled, 5'-GCTCTATGGGACGAAAGGTGAT-3') and SET (5'-ATCT-CCGTTTCTGTTCTTAAT-3') shRNA oligonucleotides, used in mESCs (Edupuganti et al., 2017), had a forward MluI site overhang and a reverse ClaI site overhang. In addition, an *NdeI* site was inserted after the terminating signal of 5 ‘T’ nucleotides to allow oligonucleotide insertion verification. Single-stranded oligonucleotides were purchased (IDT) and hybridized to make double-stranded oligonucleotides using standard hybridization procedures. Hybridized oligonucleotides were inserted into the pLVTHM vector (Addgene #12247) between MluI and ClaI sites. Lentiviral particles were prepared by transfecting pLVTHM-shSET, LV-VSVG and CMV-dr8.9-dvpr packaging plasmids (Edupuganti et al., 2017) into HEK 293T cells using Lipofectamine2000 (Invitrogen). Low passage R1 mESCs were infected with a low titer of lentiviral particles to prevent multiple integrations. Several GFP-positive colonies were picked, clonally expanded and checked for highest knockdown efficiency. All cells were routinely checked for mycoplasma contamination.

Identification of GFP–H1.2 interactors by MS

GFP–H1.2-containing protein complexes were enriched from nuclear extracts of SILAC-labeled HeLa cells stably expressing GFP–H1.2 by

immunopurification with GFP-trap beads (Chromotek) as described previously (Aydin et al., 2014). In short, GFP-H1.2-expressing or wild-type SILAC-labeled HeLa cells from six 15 cm dishes were harvested by scraping in PBS. Nuclei were isolated by resuspending cells in 2× pellet volume HEPES buffer A [10 mM HEPES pH 7.6, 1.5 mM MgCl₂, 10 mM KCl, 0.5 mM DTT and protease inhibitor cocktail (Roche)], homogenizing the cells using pestle A of a Dounce homogenizer and centrifugation for 10 min at 2100 g (3000 rpm). Nuclei were lysed in HEPES buffer B [20 mM HEPES pH 7.6, 1.5 mM MgCl₂, 150 mM NaCl, 25% glycerol, 0.5 mM DTT and protease inhibitor cocktail (Roche)] using pestle B of a Dounce homogenizer. Chromatin was fragmented with MNase (25 U, Sigma) digestion for 1 h at 4°C. Lysates were cleared by centrifugation (15 min at 16,000 g (13,000 rpm) and incubated with GFP-trap beads (Chromotek) for 4 h at 4°C. Beads were washed four times in HEPES buffer B and mixed together. Proteins were eluted with Laemmli sample buffer and loaded onto a 4–15% gradient SDS-PAGE gel (Bio-Rad). After running, the gel was fixed and stained with Roti-Blue (Carl Roth GmbH) according to the manufacturer's protocol. Gel lanes were cut into 2-mm slices using an automatic gel slicer and subjected to in-gel reduction with dithiothreitol, alkylation with iodoacetamide and digestion with trypsin (Promega, sequencing grade) (Schwertman et al., 2013). Nanoflow liquid chromatography tandem mass spectrometry (LC-MS/MS) was performed on a quadrupole Orbitrap (Q-Exactive, Thermo Fisher Scientific) mass spectrometer equipped with an EASY-nLC 1000 (Thermo Fisher Scientific). Peptide samples were loaded onto ReproSil C18 reversed phase columns (20 cm×75 µm) and eluted with a linear gradient (70 min) from 5 to 80% acetonitrile containing 0.1% formic acid at a constant flow rate of 300 nl/min. Fragmentation of the peptides was performed in a data-dependent acquisition mode. MS1 spectra were collected at a resolution of 70,000, with an automated gain control target of 10⁶ and a max injection time of 50 ms. The 10 most intense ions were selected for MS/MS. Precursors were filtered according to charge state (2–7z), and monoisotopic peak assignment. Previously interrogated precursors were dynamically excluded for 30 s. Peptide precursors were isolated with a quadrupole mass filter set to a width of 2.0 Th. MS experiments were performed in duplicate with label swap to allow easy exclusion of contaminants and to reduce false positive hits. Raw MS data was analyzed using MaxQuant software (version 1.3.0.5) (Cox et al., 2009, 2011) with protein-level false discovery rate set at 1% and minimum peptide length of 7. MS/MS spectra were searched against the human UniProt FASTA database (version 2013) using the Andromeda search engine (Cox et al., 2011). Contaminants and reverse hits were removed.

Clonogenic survival assays

Cells were seeded in six-well plates a day before treatment (U2OS and mESCs, 400 cells/well; Hct116, 250 cells/well). Cells were treated with single doses of UV-C or ionizing radiation. KBrO₃ (Sigma) and H₂O₂ (Sigma) treatments were by continuous exposure at the indicated concentrations. Mytomycin C (Kyowa) treatment was for 1 h, and hydroxyurea (HU; Sigma) and Illudin S treatments were for 24 h at the indicated concentrations. Each experiment was performed in triplicate. After 6–8 days, the colonies were fixed and stained with 50% methanol, 43% H₂O, 7% acetic acid and 0.1% Brilliant Blue R (Sigma). The number of colonies was counted using a GelCount™ (Oxford Optronix, version 1.1.2.0). The survival was plotted as the relative number of colonies after treatment compared to the number of colonies in non-treated samples.

FRAP

GFP-H1.2-expressing HeLa cells were seeded on coverslips and kept at 37°C and 5% CO₂. A Leica SP5 confocal laser scanning microscope with a 63× oil immersion objective and Leica LAS AF software was used for image acquisition. Imaging was performed at 1400 Hz with a line averaging of 2 and a 12× zoom. For FRAP analysis a strip 32 pixels wide, spanning the entire diameter of the cell nucleus was bleached using a 488 nm laser with high laser power (1 frame, 100% laser power). Recovery of the fluorescence signal was measured every 0.2 s for 200 s. Fluorescence intensity was normalized to pre-bleach values.

Immunofluorescence

Cells were grown on glass 24 mm coverslips. Cells were fixed in 2% paraformaldehyde in PBS containing 0.1% Triton X-100 and washed 2 times for 10 min in PBS with 0.1% Triton X-100 and one time in PBS with 0.15% glycine and 0.5% BSA. For 6–4PP and histone H3 staining, cells were incubated for 5 min in freshly made 0.07 M NaOH. Cells were incubated for 1–2 h with primary antibodies in PBS with 0.15% Glycine and 0.5% BSA then subsequently washed 5 times in PBS with 0.1% Triton X-100. After washing, the cells were incubated for 1–2 h with secondary antibodies in PBS with 0.15% glycine, 0.5% BSA and DAPI (0.1 µg/ml) or Sytox Green (0.5 µM, Life Technologies). Cells were washed five times in PBS containing 0.1% Triton X-100 and mounted using Aqua-Poly/Mount (Polysciences). For cytochrome *c* release assays, cells were grown in glass-bottom 96-well plates (Greiner). At 32 h before fixation, cells were UV-irradiated and the caspase inhibitor (Q-VD-OPH, 20 µM; MP Biomedicals) was added. The staining procedure described above was used and, after secondary antibody staining [anti-mouse-488 (Invitrogen A11001), anti-mouse-594 (Invitrogen A11032), anti-goat-488 (Invitrogen A11055)], cells were washed in PBS with Triton X-100, fixed with 2% paraformaldehyde and stored in PBS. Antibodies used were mouse anti-6–4PP (1:1000, Cosmo Bio, 64M2), goat anti-H3 (1:250, Santa Cruz, sc-8654), mouse anti-cytochrome *c* (1:100, BD Biosciences, 556432) and mouse anti-γ-H2AX (Ser139) (1:1000, Millipore, JWB301). Images were acquired using a Zeiss LSM700 confocal microscope equipped with a 40× oil Plan-apochromat 1.4 NA objective or (for cytochrome *c* release assays) a Leica SP5 confocal scanning microscope with a 20× HCX PL APO CS 0.7 NA objective. Images were analyzed using ImageJ software (Schindelin et al., 2012).

Western blotting

Whole-cell extracts were made by scraping cells into Laemmli buffer and boiling for 3 min. Lysates were separated on SDS-PAGE gels and transferred to PVDF membranes (0.45 µm, Millipore). Blots were blocked with 5% milk (Sigma) in PBS-Tween (PBS with 0.05% Tween 20) and incubated 1 h or overnight with primary antibodies. Blots were washed 5 times for 5 min with PBS-Tween and incubated with secondary fluorescent antibodies [anti-rabbit, CF IRDye 770 (Sigma, sab4600215), anti-rabbit, CF IRDye 680 (Sigma, sab4600200), anti-mouse, CF IRDye 770 (Sigma, sab4600214), anti-mouse, CF IRDye 680 (Sigma, sab4600199)] for 1 h, followed by another 5 washes in PBS-Tween. Blots were visualized using an Odyssey CLX Infrared Imaging System (LI-COR Biosciences). Primary antibodies used were mouse anti-γ-H2AX (Ser139) (1:1000, Millipore, JWB301), mouse anti-tubulin (1:5000, Sigma, B512), rabbit anti-SET (1:1000, Abcam, ab181990), rabbit anti-XPA (1:250, Santa Cruz, SC-853), mouse anti-KAP1 (1:1000, Abnova, H00010155-M01) and rabbit anti-H1.2 (1:1000, Abcam, ab17677).

Unscheduled DNA synthesis

C5RO cells were seeded on 24 mm coverslips and cultured in low serum (1%) medium to accumulate cells in G0 phase. Cells were irradiated with 16 J/m² UV-C and incubated for 3 h in medium containing EdU (5 µM, Invitrogen) and 5-fluorodeoxyuridine (1 µM, Sigma), followed by a 15 min chase of medium containing thymidine. Cells were fixed in 3.6% formaldehyde and permeabilized for 20 min in 0.5% Triton X-100 in PBS. Click-iT labeling reactions (Invitrogen) were performed according to manufacturer's protocol and slides were mounted using DAPI Vectashield (Vector Laboratories). Images were obtained with a Zeiss LSM700 equipped with a 40×1.3 NA oil immersion Plan apochromat objective.

Recovery of RNA synthesis

Cells were cultured on coverslips and irradiated with 6 J/m² UV-C or mock treated. Cells were incubated for 2 h in medium containing EU (20 µM, Base Click) at different timepoints after UV treatment. Cells were fixed in 3.6% formaldehyde and permeabilized in PBS containing 0.5% Triton X-100 for 20 min. Click-iT labeling reactions (Invitrogen) were performed according to manufacturer's protocol and slides were mounted using DAPI Vectashield (Vector Laboratories). Images were obtained with a Zeiss LSM700 equipped with a 40×1.3 NA oil immersion Plan apochromat objective and quantified using ImageJ software (Schindelin et al., 2012).

Cell cycle analysis

Cells were labeled with 10 μ M EdU for 15 min at 37°C to identify S-phase cells. Subsequently, cells were harvested and fixed in 1% formaldehyde for 10 min at room temperature. Cells were permeabilized with 10% saponin in PBS for 10 min on ice and a Click-iT labeling reaction was performed using the Click-iT EdU Alexa Fluor 594 flow cytometry assay kit (Invitrogen) according to the manufacturer's protocol. Cells were washed with 1% BSA in PBS and resuspended in PBS containing 0.1 mg/ml RNase and 1 μ g/ml DAPI. Cell cycle profiles were obtained by flow cytometry (LSR Fortessa, BD Biosciences). Data was analyzed using FlowJo vX.0.7 (Tree Star Inc.).

RT-qPCR

Cells were treated with 20 μ M etoposide for 24 h prior to RNA extraction. The RNeasy Plus Mini kit (Qiagen) was used to extract RNA from the cells according to the manufacturer's protocol, and cDNA was made from 500 ng RNA using Superscript III reverse transcriptase (Invitrogen) and random hexamer primers (Invitrogen, 48190011). For the qPCR, PowerUp SYBR Green Master Mix (Applied Biosystems) was mixed with cDNA and the relevant oligonucleotides. Primers used were: *CDKN1A* (encoding p21) forward, 5'-CTGAGACTCTCAGGGTCGAA-3'; *CDKN1A* reverse, 5'-C-GGCGTTTGGAGTGGTAGAA-3'; *NOXA* forward, 5'-AGAGCTGGAA-GTCGAGTGT-3'; *NOXA* reverse, 5'-GCACCTTCACATTCCTCTC-3'; *ACTB* (encoding β -actin) forward, 5'-AGAGCTACGAGCTGCCTGAC-3'; *ACTB* reverse, 5'-AGCACTGTGTGGCGTACAG-3'; *GAPDH* forward, 5'-AAATCCATGGCCACCGTCA-3'; *GAPDH* reverse, 5'-CATCG-CCCACTTGATTTT-3'; *HPRT1* forward, 5'-TATGGCGACCCGCAG-CCCT-3'; *HPRT1* reverse, 5'-CATCTCGAGCAAGACGTTCA-3'. Data was normalized to the average of the three housekeeping genes (*ACTB*, *GAPDH* and *HPRT1*) and mock conditions.

Acknowledgements

We thank Kyosuke Nagata (University of Tsukuba, Japan) for sharing the H1.2-FLAG construct. We thank the Erasmus MC optical imaging center (OIC) for help with confocal imaging and image analysis.

Competing interests

The authors declare no competing or financial interests.

Author contributions

Conceptualization: I.K.M., J.A.M.; Methodology: I.K.M., D.Z., S.T.B., D.H.D.; Investigation: I.K.M., D.Z., S.T.B.; Resources: P.J.V., R.R.E., E.M.; Writing - original draft: I.K.M.; Writing - review & editing: J.A.M.; Supervision: E.M., J.A.A.D., J.A.M.; Funding acquisition: J.A.M.

Funding

This work was contributed to by members of the Oncode Institute, which is partly financed by the Dutch Cancer Society (KWF Kankerbestrijding). This work was supported by the Dutch Organization for Scientific Research (Nederlandse Organisatie voor Wetenschappelijk Onderzoek) TOP Grants of Earth and Life Sciences and ZonMw (854.11.002 and 912.12.132) and Dutch Organization for Scientific Research (Nederlandse Organisatie voor Wetenschappelijk Onderzoek) VIDI grant (846.13.004).

Supplementary information

Supplementary information available online at <http://jcs.biologists.org/lookup/doi/10.1242/jcs.235473.supplemental>

References

- Adam, S., Polo, S. E. and Almouzni, G. (2013). Transcription recovery after DNA damage requires chromatin priming by the H3.3 histone chaperone HIRA. *Cell* **155**, 94-106. doi:10.1016/j.cell.2013.08.029
- Arnold, H. K. and Sears, R. C. (2008). A tumor suppressor role for PP2A-B56alpha through negative regulation of c-Myc and other key oncoproteins. *Cancer Metastasis Rev.* **27**, 147-158. doi:10.1007/s10555-008-9128-9
- Aydin, Ö. Z., Martijn, J. A., Ribeiro-Silva, C., Rodríguez, López, A., Wijgers, N., Smeenk, G., van Attikum, H., Poot, R. A., Vermeulen, W. et al. (2014). Human ISWI complexes are targeted by SMARCA5 ATPase and SLIDE domains to help resolve lesion-stalled transcription. *Nucleic Acids Res.* **42**, 8473-8485. doi:10.1093/nar/gku565
- Beuzer, P., Quivy, J.-P. and Almouzni, G. (2014). Establishment of a replication fork barrier following induction of DNA binding in mammalian cells. *Cell Cycle* **13**, 1607-1616. doi:10.4161/cc.28627
- Block, W. D., Merkle, D., Meek, K. and Lees-Miller, S. P. (2004). Selective inhibition of the DNA-dependent protein kinase (DNA-PK) by the radiosensitizing agent caffeine. *Nucleic Acids Res.* **32**, 1967-1972. doi:10.1093/nar/gkh508
- Campeau, E., Ruhl, V. E., Rodier, F., Smith, C. L., Rahmberg, B. L., Fuss, J. O., Campisi, J., Yaswen, P., Cooper, P. K. and Kaufman, P. D. (2009). A versatile viral system for expression and depletion of proteins in mammalian cells. *PLoS ONE* **4**, e6529. doi:10.1371/journal.pone.0006529
- Christensen, D. J., Chen, Y., Oddo, J., Matta, K. M., Neil, J., Davis, E. D., Volkheimer, A. D., Lanasa, M. C., Friedman, D. R., Goodman, B. K. et al. (2011). SET oncoprotein overexpression in B-cell chronic lymphocytic leukemia and non-Hodgkin lymphoma: a predictor of aggressive disease and a new treatment target. *Blood* **118**, 4150-4158. doi:10.1182/blood-2011-04-351072
- Clouaire, T., Rocher, V., Lashgari, A., Arnould, C., Aguirrebengoa, M., Biernacka, A., Skrzypczak, M., Aymard, F., Fongang, B., Dojer, N. et al. (2018). Comprehensive mapping of histone modifications at DNA double-strand breaks deciphers repair pathway chromatin signatures. *Mol. Cell* **72**, 250-262.e6. doi:10.1016/j.molcel.2018.08.020
- Cox, J., Matic, I., Hilger, M., Nagaraj, N., Selbach, M., Olsen, J. V. and Mann, M. (2009). A practical guide to the MaxQuant computational platform for SILAC-based quantitative proteomics. *Nat. Protoc.* **4**, 698-705. doi:10.1038/nprot.2009.36
- Cox, J., Neuhauser, N., Michalski, A., Scheltema, R. A., Olsen, J. V. and Mann, M. (2011). Andromeda: a peptide search engine integrated into the MaxQuant environment. *J. Proteome Res.* **10**, 1794-1805. doi:10.1021/pr101065j
- Dinant, C., Ampatzidis-Michailidis, G., Lans, H., Tresini, M., Lagarou, A., Grosbart, M., Theil, A. F., van Cappellen, W. A., Kimura, H., Bartek, J. et al. (2013). Enhanced chromatin dynamics by FACT promotes transcriptional restart after UV-induced DNA damage. *Mol. Cell* **51**, 469-479. doi:10.1016/j.molcel.2013.08.007
- Dunkern, T. R., Fritz, G. and Kaina, B. (2001). Ultraviolet light-induced DNA damage triggers apoptosis in nucleotide excision repair-deficient cells via Bcl-2 decline and caspase-3/8 activation. *Oncogene* **20**, 6026-6038. doi:10.1038/sj.onc.1204754
- Edupuganti, R. R., Harikumar, A., Aaronson, Y., Biran, A., Sailaja, B. S., Nissim-Rafinia, M., Azad, G. K., Cohen, M. A., Park, J. E., Shivallia, C. S. et al. (2017). Alternative SET/TAFI promoters regulate embryonic stem cell differentiation. *Stem Cell Rep.* **9**, 1291-1303. doi:10.1016/j.stemcr.2017.08.021
- Escargueil, A. E., Soares, D. G., Salvador, M., Larsen, A. K. and Henriques, J. A. (2008). What histone code for DNA repair? *Mutat. Res.* **658**, 259-270. doi:10.1016/j.mrev.2008.01.004
- Fagbemi, A. F., Orelli, B. and Schärer, O. D. (2011). Regulation of endonuclease activity in human nucleotide excision repair. *DNA Repair* **10**, 722-729. doi:10.1016/j.dnarep.2011.04.022
- Fan, Z., Beresford, P. J., Oh, D. Y., Zhang, D. and Lieberman, J. (2003). Tumor suppressor NM23-H1 is a granzyme A-activated DNase during CTL-mediated apoptosis, and the nucleosome assembly protein SET is its inhibitor. *Cell* **112**, 659-672. doi:10.1016/S0092-8674(03)00150-8
- Gamble, M. J., Erdjument-Bromage, H., Tempst, P., Freedman, L. P. and Fisher, R. P. (2005). The histone chaperone taf-i/set/inhat is required for transcription in vitro of chromatin templates. *Mol. Cell Biol.* **25**, 797-807. doi:10.1128/MCB.25.2.797-807.2005
- Guleria, A. and Chandna, S. (2016). ATM kinase: much more than a DNA damage responsive protein. *DNA Repair* **39**, 1-20. doi:10.1016/j.dnarep.2015.12.009
- Hanasoge, S. and Ljungman, M. (2007). H2AX phosphorylation after UV irradiation is triggered by DNA repair intermediates and is mediated by the ATR kinase. *Carcinogenesis* **28**, 2298-2304. doi:10.1093/carcin/bgm157
- Hoeijmakers, J. H. J. (2001). Genome maintenance mechanisms for preventing cancer. *Nature* **411**, 366-374. doi:10.1038/35077232
- Hoeijmakers, J. H. J. (2009). DNA damage, aging, and cancer. *N. Engl. J. Med.* **361**, 1475-1485. doi:10.1056/NEJMra0804615
- Hung, M.-H. and Chen, K.-F. (2017). Reprogramming the oncogenic response: SET protein as a potential therapeutic target in cancer. *Expert Opin Ther. Targets* **21**, 685-694. doi:10.1080/14728222.2017.1336226
- Jackson, S. P. and Bartek, J. (2009). The DNA-damage response in human biology and disease. *Nature* **461**, 1071-1078. doi:10.1038/nature08467
- Janicki, S. M., Tsukamoto, T., Salghetti, S. E., Tansey, W. P., Sachidanandam, R., Prasanth, K. V., Ried, T., Shav-Tal, Y., Bertrand, E., Singer, R. H. et al. (2004). From silencing to gene expression: real-time analysis in single cells. *Cell* **116**, 683-698. doi:10.1016/S0092-8674(04)00171-0
- Kalouisi, A., Hoffbeck, A.-S., Selemenakis, P. N., Pinder, J., Savage, K. I., Khanna, K. K., Brino, L., Delleire, G., Gorgoulis, V. G. and Soutoglou, E. (2015). The nuclear oncogene SET controls DNA repair by KAP1 and HP1 retention to chromatin. *Cell Rep.* **11**, 149-163. doi:10.1016/j.celrep.2015.03.005
- Kato, K., Okuwaki, M. and Nagata, K. (2011). Role of template activating factor-I as a chaperone in linker histone dynamics. *J. Cell Sci.* **124**, 3254-3265. doi:10.1242/jcs.083139
- Kim, J.-Y., Lee, K.-S., Seol, J.-E., Yu, K., Chakravarti, D. and Seo, S.-B. (2012). Inhibition of p53 acetylation by INHAT subunit SET/TAF-Ibeta represses p53 activity. *Nucleic Acids Res.* **40**, 75-87. doi:10.1093/nar/gkr614

- Kimura, H. and Cook, P.R.** (2001). Kinetics of core histones in living human cells: little exchange of H3 and H4 and some rapid exchange of H2B. *J. Cell Biol.* **153**, 1341-1353. doi:10.1083/jcb.153.7.1341
- Lans, H., Marteiijn, J. A. and Vermeulen, W.** (2012). ATP-dependent chromatin remodeling in the DNA-damage response. *Epigenetics Chromatin* **5**, 4. doi:10.1186/1756-8935-5-4
- Li, M., Guo, H. and Damuni, Z.** (1995). Purification and characterization of two potent heat-stable protein inhibitors of protein phosphatase 2A from bovine kidney. *Biochemistry* **34**, 1988-1996. doi:10.1021/bi00006a020
- Li, C.-L., Golebiowski, F. M., Onishi, Y., Samara, N. L., Sugawara, K. and Yang, W.** (2015). Tripartite DNA lesion recognition and verification by XPC, TFIIH, and XPA in nucleotide excision repair. *Mol. Cell* **59**, 1025-1034. doi:10.1016/j.molcel.2015.08.012
- Lieberman, H. B., Panigrahi, S. K., Hopkins, K. M., Wang, L. and Broustas, C. G.** (2017). p53 and RAD9, the DNA damage response, and regulation of transcription networks. *Radiat. Res.* **187**, 424-432. doi:10.1667/RR003CC.1
- Limsirichaikul, S., Niimi, A., Fawcett, H., Lehmann, A., Yamashita, S. and Ogi, T.** (2009). A rapid non-radioactive technique for measurement of repair synthesis in primary human fibroblasts by incorporation of ethynyl deoxyuridine (EdU). *Nucleic Acids Res.* **37**, e31. doi:10.1093/nar/gkp023
- Loven, M. A., Muster, N., Yates, J. R. and Nardulli, A. M.** (2003). A novel estrogen receptor alpha-associated protein, template-activating factor ibeta, inhibits acetylation and transactivation. *Mol. Endocrinol.* **17**, 67-78. doi:10.1210/me.2002-0280
- Mandemaker, I. K., Vermeulen, W. and Marteiijn, J. A.** (2014). Gearing up chromatin: a role for chromatin remodeling during the transcriptional restart upon DNA damage. *Nucleus* **5**, 203-210. doi:10.4161/nucl.29085
- Mandemaker, I. K., van Cuijk, L., Janssens, R. C., Lans, H., Bezstarosti, K., Hoeijmakers, J. H., Demmers, J. A., Vermeulen, W. and Marteiijn, J. A.** (2017). DNA damage-induced histone H1 ubiquitylation is mediated by HUWE1 and stimulates the RNF8-RNF168 pathway. *Sci. Rep.* **7**, 15353. doi:10.1038/s41598-017-15194-y
- Marteijn, J. A., Bekker-Jensen, S., Mailand, N., Lans, H., Schwertman, P., Gourdin, A. M., Dantuma, N. P., Lukas, J. and Vermeulen, W.** (2009). Nucleotide excision repair-induced H2A ubiquitination is dependent on MDC1 and RNF8 and reveals a universal DNA damage response. *J. Cell Biol.* **186**, 835-847. doi:10.1083/jcb.200902150
- Marteijn, J. A., Hoeijmakers, J. H. J. and Vermeulen, W.** (2015). Check, check ... triple check: multi-step DNA lesion identification by nucleotide excision repair. *Mol. Cell* **59**, 885-886. doi:10.1016/j.molcel.2015.09.007
- Mogi, S. and Oh, D. H.** (2006). gamma-H2AX formation in response to interstrand crosslinks requires XPF in human cells. *DNA Repair* **5**, 731-740. doi:10.1016/j.dnarep.2006.03.009
- Murga, M., Jaco, I., Fan, Y., Soria, R., Martinez-Pastor, B., Cuadrado, M., Yang, S.-M., Blasco, M. A., Skoutchii, A. I. and Fernandez-Capetillo, O.** (2007). Global chromatin compaction limits the strength of the DNA damage response. *J. Cell Biol.* **178**, 1101-1108. doi:10.1083/jcb.200704140
- Nakazawa, Y., Yamashita, S., Lehmann, A. R. and Ogi, T.** (2010). A semi-automated non-radioactive system for measuring recovery of RNA synthesis and unscheduled DNA synthesis using ethynyluracil derivatives. *DNA Repair* **9**, 506-516. doi:10.1016/j.dnarep.2010.01.015
- Nishiyama, M., Oshikawa, K., Tsukada, Y.-I., Nakagawa, T., Iemura, S.-I., Natsume, T., Fan, Y., Kikuchi, A., Skoutchii, A. I. and Nakayama, K. I.** (2009). CHD8 suppresses p53-mediated apoptosis through histone H1 recruitment during early embryogenesis. *Nat. Cell Biol.* **11**, 172-182. doi:10.1038/ncb1831
- Ogi, T., Limsirichaikul, S., Overmeer, R. M., Volker, M., Takenaka, K., Cloney, R., Nakazawa, Y., Niimi, A., Miki, Y., Jaspers, N. G. et al.** (2010). Three DNA polymerases, recruited by different mechanisms, carry out NER repair synthesis in human cells. *Mol. Cell* **37**, 714-727. doi:10.1016/j.molcel.2010.02.009
- Oksenyich, V. and Coin, F.** (2010). The long unwinding road: XPB and XPD helicases in damaged DNA opening. *Cell Cycle* **9**, 90-96. doi:10.4161/cc.9.1.10267
- Okuwaki, M. and Nagata, K.** (1998). Template activating factor-i remodels the chromatin structure and stimulates transcription from the chromatin template. *J. Biol. Chem.* **273**, 34511-34518. doi:10.1074/jbc.273.51.34511
- Park, J.-H., Park, E.-J., Lee, H.-S., Kim, S. J., Hur, S.-K., Imbalzano, A. N. and Kwon, J.** (2006). Mammalian SWI/SNF complexes facilitate DNA double-strand break repair by promoting gamma-H2AX induction. *EMBO J.* **25**, 3986-3997. doi:10.1038/sj.emboj.7601291
- Peterson, C and Legerski, R** (1991). High-frequency transformation of human repair-deficient cell lines by an Epstein-Barr virus-based cDNA expression vector. *Gene* **107**, 279-284. doi:10.1016/0378-1119(91)90328-9
- Polo, S. E. and Almouzni, G.** (2015). Chromatin dynamics after DNA damage: the legacy of the access-repair-restore model. *DNA Repair* **36**, 114-121. doi:10.1016/j.dnarep.2015.09.014
- Riley, T., Sontag, E., Chen, P. and Levine, A.** (2008). Transcriptional control of human p53-regulated genes. *Nat. Rev. Mol. Cell Biol.* **9**, 402-412. doi:10.1038/nrm2395
- Rogakou, E. P., Pilch, D. R., Orr, A. H., Ivanova, V. S. and Bonner, W. M.** (1998). DNA double-stranded breaks induce histone H2AX phosphorylation on serine 139. *J. Biol. Chem.* **273**, 5858-5868. doi:10.1074/jbc.273.10.5858
- Rommelaere, J. and Errera, M.** (1972). The Effect of Caffeine on the Survival of U.V.-irradiated diploid and tetraploid Chinese-hamster Cells. *Int. J. Radiat. Biol. Relat. Stud. Phys. Chem. Med.* **22**, 285-291. doi:10.1080/09553007214551061
- Sarkaria, J. N., Busby, E. C., Tibbetts, R. S., Roos, P., Taya, Y., Karnitz, L. M. and Abraham, R. T.** (1999). Inhibition of ATM and ATR kinase activities by the radiosensitizing agent, caffeine. *Cancer Res.* **59**, 4375-4382.
- Schindelin, J., Arganda-Carreras, I., Frise, E., Kaynig, V., Longair, M., Pietzsch, T., Preibisch, S., Rueden, C., Saalfeld, S., Schmid, B. et al.** (2012). Fiji: an open-source platform for biological-image analysis. *Nat. Methods* **9**, 676-682. doi:10.1038/nmeth.2019
- Schwertman, P., Bezstarosti, K., Laffeber, C., Vermeulen, W., Demmers, J. A. A. and Marteiijn, J. A.** (2013). An immunoprecipitation method for the proteomic analysis of ubiquitinated protein complexes. *Anal. Biochem.* **440**, 227-236. doi:10.1016/j.ab.2013.05.020
- Sellou, H., Lebeauupin, T., Chapuis, C., Smith, R., Hegele, A., Singh, H. R., Kozlowski, M., Bultmann, S., Ladurner, A. G., Timinsky, G. et al.** (2016). The poly(ADP-ribose)-dependent chromatin remodeler Alc1 induces local chromatin relaxation upon DNA damage. *Mol. Biol. Cell* **27**, 3791-3799. doi:10.1091/mbc.E16-05-0269
- Seo, S.-B., McNamara, P., Heo, S., Turner, A., Lane, W. S. and Chakravarti, D.** (2001). Regulation of histone acetylation and transcription by inhat, a human cellular complex containing the set oncoprotein. *Cell* **104**, 119-130. doi:10.1016/S0092-8674(01)00196-9
- Sirbu, B. M. and Cortez, D.** (2013). DNA damage response: three levels of DNA repair regulation. *Cold Spring Harb. Perspect. Biol.* **5**, a012724. doi:10.1101/cshperspect.a012724
- Smerdon, M. J.** (1991). DNA repair and the role of chromatin structure. *Curr. Opin. Cell Biol.* **3**, 422-428. doi:10.1016/0955-0674(91)90069-B
- Soria, G., Polo, S. E. and Almouzni, G.** (2012). Prime, repair, restore: the active role of chromatin in the DNA damage response. *Mol. Cell* **46**, 722-734. doi:10.1016/j.molcel.2012.06.002
- Strickfaden, H., McDonald, D., Kruhlak, M. J., Haince, J.-F., Th'ng, J. PH., Rouleau, M., Ishibashi, T., Corry, G. N., Ausio, J., Underhill, D. A. et al.** (2016). Poly(ADP-ribose)ylation-dependent transient chromatin decondensation and histone displacement following laser microirradiation. *J. Biol. Chem.* **291**, 1789-1802. doi:10.1074/jbc.M115.694992
- Sugawara, K.** (2016). Molecular mechanisms of DNA damage recognition for mammalian nucleotide excision repair. *DNA Repair* **44**, 110-117. doi:10.1016/j.dnarep.2016.05.015
- Thorslund, T., Ripplinger, A., Hoffmann, S., Wild, T., Uckelmann, M., Villumsen, B., Narita, T., Sixma, T. K., Choudhary, C., Bekker-Jensen, S. et al.** (2015). Histone H1 couples initiation and amplification of ubiquitin signalling after DNA damage. *Nature* **527**, 389-393. doi:10.1038/nature15401
- Verschure, P.J., van der Kraan, I., de Leeuw, W., van der Vlag, J., Carpenter, A.E., Belmont, A.S. and van Driel, R.** (2005). In vivo HP1 targeting causes large-scale chromatin condensation and enhanced histone lysine methylation. *Mol. Cell Biol.* **25**, 4552-4564. doi:10.1128/MCB.25.11.4552-4564.2005
- Wang, D., Kon, N., Lasso, G., Jiang, L., Leng, W., Zhu, W.-G., Qin, J., Honig, B. and Gu, W.** (2016). Acetylation-regulated interaction between p53 and SET reveals a widespread regulatory mode. *Nature* **538**, 118-122. doi:10.1038/nature19759
- Ward, I. M. and Chen, J.** (2001). Histone H2AX is phosphorylated in an ATR-dependent manner in response to replicational stress. *J. Biol. Chem.* **276**, 47759-47762. doi:10.1074/jbc.C100569200
- Yuan, J., Adamski, R. and Chen, J.** (2010). Focus on histone variant H2AX: to be or not to be. *FEBS Lett.* **584**, 3717-3724. doi:10.1016/j.febslet.2010.05.021
- Zhang, Q., Giebler, H. A., Isaacson, M. K. and Nyborg, J. K.** (2015). Eviction of linker histone H1 by NAP-family histone chaperones enhances activated transcription. *Epigenetics Chromatin* **8**, 30. doi:10.1186/s13072-015-0022-8
- Zhang, Y., Qian, D., Li, Z., Huang, Y., Wu, Q., Ru, G., Chen, M. and Wang, B.** (2016). Oxidative stress-induced DNA damage of mouse zygotes triggers G2/M checkpoint and phosphorylates Cdc25 and Cdc2. *Cell Stress Chaperones* **21**, 687-696. doi:10.1007/s12192-016-0693-5